Dual-Band Polarization Control with Pairwise Positioning of Polarization Singularities in Metasurfaces

Chloe F. Doiron,* Igal Brener,† and Alexander Cerjan‡
Center for Integrated Nanotechnologies, Sandia National Laboratories
1515 Eubank SE, Albuquerque, New Mexico 87123, USA

(Received 25 January 2024; revised 25 July 2024; accepted 11 October 2024; published 22 November 2024)

Emerging applications of metasurfaces in classical and quantum optics are driving the need for precise polarization control of nearly-degenerate, high quality (Q)-factor modes. However, current approaches to creating specifically polarized pairs of modes force a trade-off between maintaining high Q factors and robustness. Here, we solve this challenge by employing pairwise generation, annihilation, and positioning of polarization singularities, derived from symmetry-guaranteed pairs of symmetry-protected bound states in the continuum. We experimentally demonstrate this design paradigm in silicon metasurfaces with mode splittings of ≈20 nm, mode splitting deviations as low as 1 nm, and Q factors up to 200. This approach opens new avenues for enhancing metasurface performance across a diverse range of applications, including sensing, modulating, nonlinear mixing, and generating quantum light.

DOI: 10.1103/PhysRevLett.133.213802

Controlling the far-field polarization response of a metasurface is critical for a variety of applications in classical and quantum optics [1–4]. While polarization control can be achieved through careful design of out-coupling rates and phases for two orthogonal directions (i.e., s- and p-), new applications of metasurfaces are driving the creation of increasingly sophisticated devices that require multidimensional control extending beyond polarization. In particular, one emerging need is the ability to robustly create and control nearly-degenerate pairs of high-Q modes while simultaneously shaping the polarization responses. Achieving such comprehensive control would create pathways for enhancing metasurfaces in applications ranging from narrowband, polarization independent sensors [5–8] and modulators [9] to entangled photon-pair sources [10–12] with orthogonality across the Poincaré sphere, as well as nearly degenerate nonlinear mixers [13–16].

Fundamentally, achieving predictable multidimensional control over metasurface responses stems from the generally smooth variation of a metasurface's properties as the system is altered. As such, singularities, where a system's properties undergo a discontinuous change, play an outsized role in determining metasurface properties, effectively dictating a system's response over a broad range of parameter space. Indeed, metasurface singularities have been used to control resonance lifetimes [17], non-Hermitian responses [18], disordered media responses [19], and degeneracies [20]. Moreover, because singularities obey conservation requirements (Poincaré–Hopf theorem [21–23]), they provide protection against perturbations from material and fabrication imperfections; thus, realizing robust, simultaneous control over a metasurface's Q-factor and polarization amounts to simultaneously controlling the singularities of each property. As Q factors are necessarily positive scalars, a Q-factor singularity is a location in parameter space where $Q \to \infty$, i.e., where the system exhibits a bound state in the continuum (BIC) [24]. Due to the smooth variation of Q away from the singularity, a system can exhibit arbitrarily large Q factors in the vicinity of a BIC, yielding a design space for creating quasi-BICs with any specified lifetime. Similarly, a metasurface's polarization response (at a given wave vector) is specified by the polarization ellipse, whose major axis determines the orientation of polarization ellipse. As such, polarization can exhibit many forms of singularities: BICs, where the ellipse's major and minor axes both have zero length indicating the state does not radiate [24]; C points, where the ellipse's major and minor axes have the same, nonzero length, yielding an undefinable ellipse orientation and indicating a circularly polarized response [25–27]; and band degeneracies, where there is no well-defined polarization for either resonance band [20].

Previously, concurrent control over both Q and polarization singularities enabled the creation of metasurfaces to generate non-zero orbital angular momentum [28–31], lasing with near-perfect circular polarization [32], and shaping narrowband wavefronts [33–37]. However, the design approaches these previous works use are only applicable to single resonance bands and therefore only enable control over spectrally isolated singularities. Prior studies considering

*Contact author: cfdoiro@sandia.gov
†Contact author: ibrener@sandia.gov
‡Contact author: awcerja@sandia.gov

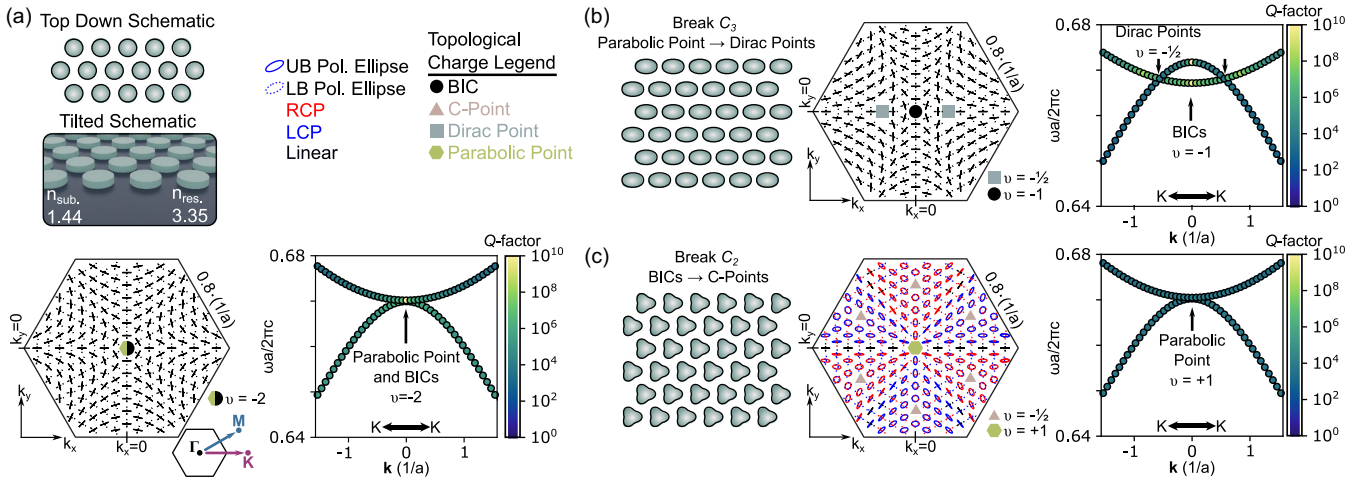

FIG. 1. (a) Symmetry-guaranteed pairs of symmetry-protected BICs can form when all symmetries of the triangular lattice are preserved. Looking at the eigenpolarization and band structure (normalized frequency units $(\omega a/2\pi c)$) near the $\mathbf{\Gamma}$ point, a topological singularity exists at the $\mathbf{\Gamma}$ point due to the degenerate BICs, with topological charge $\nu = -2$. (b) When a C_3 symmetry breaking deformation (ζ) is applied to the resonators in the triangular lattice, the degeneracy is lifted resulting in the creation of two Dirac points away from the $\mathbf{\Gamma}$ point with $\nu = -\frac{1}{2}$ each, but two symmetry-protected BICs remain at the $\mathbf{\Gamma}$ point with $\nu = -1$. (c) When a C_2 symmetry breaking deformation (δ) is applied, the parabolic degeneracy (now with $\nu = +1$) is preserved and the symmetry-protected BICs are converted to quasi-BICs, resulting in the creation of 6 C points per band with $\nu = -\frac{1}{2}$ each.

multiband phenomena overcame the lack of Q-factor singularities near band degeneracies [20,38,39] by relying on fine tuning accidental degeneracies of BICs [11,40,41] or C points [42]. Unfortunately, these fine-tuning approaches yield bands that are unpredictable under perturbations, resulting in metasurfaces susceptible to fabrication and material imperfections [43–45], and therefore are incompatible with applications where robust dual-band control is necessary.

Here, we experimentally demonstrate robust, simultaneous control over the polarization and Q-factor singularities of two nearly degenerate metasurface resonances. To do so, we build a design framework rooted in system symmetries—using symmetry to guarantee the formation of degenerate pairs of symmetry-protected BICs. As we show, through judicious symmetry breaking we can generate, annihilate, and position polarization singularities arising from BICs and band degeneracies. Moreover, a symmetry-based approach enables marked robustness, highlighted by our experimental demonstration of polarization control through pairwise rotation of singularities with a mode splitting deviation of 1 nm, representing a fractional variation less than 1×10^{-3} from the designed central resonance wavelength without structural fine tuning. Looking forward, as our design method is underpinned by pairwise control of singularities, it has broad applicability, from enabling narrowband metasurfaces operating as Poincaré sphere spanning polarizers in scattering configurations, to developing high-Q metasurfaces enhancing light generation (nonlinear, thermal, and spontaneous) while shaping far-field polarization properties of emission. Moreover, since our approach is rooted in group theory, it is translatable to controlling pairs of singularities in acoustic, mechanical, and optomechanical systems [46,47].

To demonstrate pairwise polarization singularity manipulation across two resonance bands, we consider an all-dielectric metasurface comprised of a triangular lattice of finite-thickness silicon resonators ($n \approx 3.35$) surrounded by air on a fused silica substrate ($n \approx 1.44$), and calculate its resonance band structure, Bloch eigenstates, and corresponding eigenpolarizations (far-field polarization states of the eigenstates of the metasurface resonances; see Supplemental Material [48]) using guided-mode expansion (legume, guided mode expansion implementation [52]). The resonators of the symmetry-preserved structure are cylinders with height $0.2a$ and radius $0.45a$, where a is the lattice constant. By starting with a triangular array of cylinders, all of the rotational symmetries of the underlying structure's C_{6v} symmetry are preserved [53]. For two of the metasurface's resonance bands [Fig. 1(a)], calculations show that at the $\mathbf{\Gamma}$ point (normal incidence, i.e., with in-plane wave vector $\mathbf{k}_{\|} = (0, 0)$) the two bands exhibit a parabolic degeneracy and Q factors $> 10^{10} \approx \infty$, indicating the presence of BICs [55]. Together, these features show that the modes at $\mathbf{\Gamma}$ belong to the E_2 irreducible representation of C_{6v} [56], i.e., a pair of degenerate modes in a triangular reflection-symmetric lattice that are even with respect to 180° rotational symmetry and therefore forbidden from radiating to the far field.

As the two modes in Fig. 1(a) are degenerate and have infinite Q factors at $\mathbf{\Gamma}$, they necessarily possess polarization singularities at $\mathbf{\Gamma}$. The topological charge of these

polarization singularities can be determined from the winding number of the major axis of the polarization ellipse around the singularity following a closed path D [24,27,57],

$$\nu = \frac{1}{2\pi}\oint_D d\mathbf{k}_{\parallel} \cdot \nabla_{\mathbf{k}_{\parallel}} \rho(\mathbf{k}_{\parallel}). \tag{1}$$

Here, the angle of the polarization ellipse $\rho(\mathbf{k}_{\parallel})$ is calculated by projecting the eigenpolarization ellipse onto the xy plane. When all symmetries are preserved, the eigenpolarizations in Fig. 1(a) show that these polarization singularities possess a topological charge $\nu = -2$ at the $\mathbf{\Gamma}$ point for both upper and lower bands (see Supplemental Material [48] for separated eigenpolarization plots). This can be visually verified by inspecting the winding of the polarization ellipses about a closed path D that contains the singularities.

While there are many approaches to controlling singularities, group theory provides an intuitive framework for controlling singularities since the symmetry of the modes is determined by irreducible representations with physically meaningful characters. If C_{6v} symmetry is preserved, the Q-factor and polarization singularities of the pair of metasurface resonance bands in Fig. 1(a) must remain colocated, even in the presence of higher order perturbations so long as they possess C_6 rotational symmetry. However, these two types of singularities are protected by different underlying lattice symmetries: the Q-factor singularity is protected at $\mathbf{\Gamma}$ by C_2 (180°) rotational symmetry, while the polarization singularity due to the band degeneracy is protected at $\mathbf{\Gamma}$ by C_3 (120°) rotational symmetry [47,58]. Thus, as C_2 and C_3 are independent subgroups of C_{6v}, either rotational symmetry can be broken or preserved without affecting the other through changes to the system's geometry, yielding two independent mechanisms for controlling the system's singularities. In particular, after breaking a protecting symmetry, polarization singularities are allowed to undergo pairwise annihilation, creation, and conversion events in both bands. While the exact dynamics depend on the specific symmetry breaking perturbations, the total topological charge must be conserved ($\sum \nu$) as required by the Poincaré–Hopf theorem [21–23].

As an example, consider a general alteration to the radius of the cylindrical resonators as

$$r(\theta) = r_0 + \zeta \cos(2m[\theta + \varphi]) + \delta \cos(3m[\theta + \psi]). \tag{2}$$

Here, the radial profile ($r(\theta)$) depends on the base radius (r_0) and symmetry breaking strengths with ζ determining the strength of 120° (C_3) symmetry breaking and δ dictating the strength of 180° (C_2) symmetry breaking.

When 120° rotation symmetry (C_3) is broken with $\zeta = 5 \times 10^{-3} a$, the degenerate BICs become nondegenerate BICs with infinite Q factors and nonzero splitting [Fig. 1(b)]. The symmetry reduction destroys the parabolic point degeneracy resulting in the creation of two Dirac

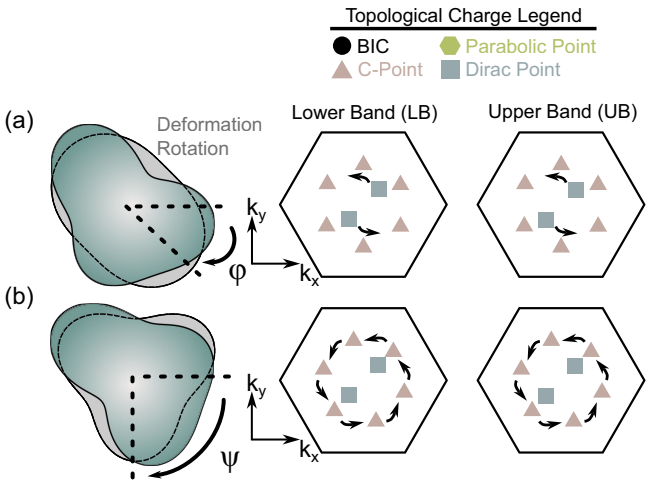

FIG. 2. (a) By rotating the C_3 symmetry breaking deformation (φ), the angular positions of the Dirac points and the corresponding polarization singularities for both bands can be controlled. (b) The angular positions of the C points for both bands can be controlled by rotating the C_2 symmetry breaking deformation ψ.

point degeneracies each with charge $\nu = -\frac{1}{2}$. These points are created near the $\mathbf{\Gamma}$ point with the radial position determined by the C_3 symmetry breaking strength. As evidenced by the Q factors and eigenpolarizations, BICs, and thus polarization singularities, are still present at the $\mathbf{\Gamma}$ point with a topological charge of $\nu = -1$ for each band. As required, the total topological charge is conserved with $\sum \nu = -2$, which can be visually verified by inspecting the winding of the polarization ellipses for a path encircling the BICs and Dirac points in Fig. 1(b).

Similarly, when 180° rotational symmetry (C_2) is broken with $\delta = 5 \times 10^{-3} a$, the degenerate BICs become degenerate quasi-BICs [Fig. 1(c)] with finite Q factors. The infinite Q factors at $\mathbf{\Gamma}$ are now finite with Q factors of 6.6×10^4 and 6.8×10^4 for the lower and upper bands, respectively. This symmetry reduction results not only in destruction of the BIC but also the formation of six new C-point polarization singularities, each with topological charge $\nu = -\frac{1}{2}$, where the eigenpolarization is circular; three left-handed and three right-handed per band. The parabolic degeneracy is still present, but with a topological charge $\nu = +1$, which can be verified by seeing that the polarization ellipse rotates clockwise along a clockwise path encircling the degeneracy. As required, the total topological charge ($\sum \nu = -2$) is conserved.

Beyond creating or annihilating singularities, full control requires a mechanism for performing an in-plane rotation of the underlying singularities. Rotating the 120° symmetry breaking deformation results in a new silicon resonator profile and angular rotation of only the Dirac points [Fig. 2(a)]. Correspondingly, rotating the 180° symmetry breaking deformations yields a new silicon resonator profile and angular rotation of only the C points [Fig. 2(b)].

To experimentally demonstrate independent rotational control, we fabricated a series of silicon metasurfaces on a single fused silica substrate with height 200 nm, base radius 400 nm, and periodicity 1000 nm [Fig. 3(a)]. To break C_2 and C_3 symmetries we used symmetry breaking strengths of $\delta = 25$ nm and $\zeta = 30$ nm, respectively. Compared to simulations, we chose larger symmetry breaking strengths to increase mode splitting and visibility of reflectance peaks. At the $\mathbf{\Gamma}$ point, the eigenpolarizations for the upper and lower bands are linear and orthogonal with singularity positions determining the angle of the eigenpolarization (see Supplemental Material [48]). By illuminating with a fixed linear polarization and rotating the symmetry deformation, the orientation of the eigenpolarizations can be tracked from the mode coupling efficiency through reflectance peak amplitudes with $|R_{\text{peak}} - R_{\text{background}}| \propto \cos^2(\alpha)$, where α is the angle between input light polarization and the eigenpolarization major axis (see Supplemental Material). We illuminated the metasurfaces with linearly polarized light polarized parallel to nearest neighbors. When the C_2 and C_3 symmetry breaking deformation angles ψ and φ in Eq. (2) are both 0°, the polarization of the incident light is parallel to the major axis of the upper band eigenpolarization and perpendicular to the major axis of the lower band eigenpolarization. In reflectance measurements, this results in the resonance from the upper band being visible near 1550 nm while that of the lower band is barely observed in Fig. 3(c).

As the symmetry breaking deformation angle increases, the amplitude of upper band resonance decreases [Figs. 3(c) and 3(d)] while the amplitude of the lower band resonance increases until a rotation angle of 90°, where the lower band resonance's amplitude response is maximized compared to the minimized upper band resonance. When the C_3 symmetry breaking deformation angle reaches 90°, the Dirac points have rotated 90° [Fig. 3(b)]. Beyond 90° deformation angles, the lower band resonance amplitude decreases while the amplitude of the upper band resonance increases until 180° where the lower band is minimized and the upper band is maximized. Physically, this swapping corresponds to the condition where the two Dirac points have exchanged positions from the starting scenario (0° deformation angle). The experimental results are in good agreement with predictions from eigenpolarization simulations [Fig. 3(d)].

Likewise, when the angle of C_2 symmetry breaking deformation is rotated polarization is controlled—but now arising from the movement of C points in the upper and lower bands. Scanning electron micrographs of the fabricated metasurfaces and the corresponding reflectance measurements for a range of C_2 symmetry breaking deformation angles are presented in Fig. 4(a). When rotating the C_2 symmetry breaking deformation, orthogonal eigenpolarizations occur when the deformation angle reaches 30° [Fig. 3(c)]. Increasing the angle to 60° causes the initial polarization responses to reappear, corresponding

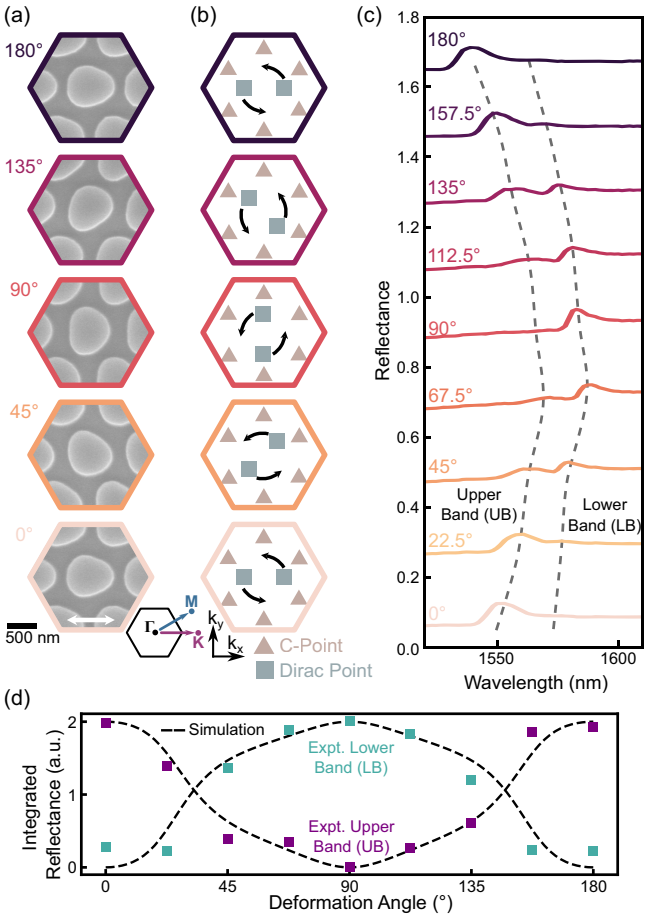

FIG. 3. (a) Scanning electron micrographs of fabricated metasurfaces and (b) schematic denoting the movement of Dirac points when the C_3 symmetry breaking deformation angle (φ) is swept from 0° to 180°. (c) Corresponding experimentally measured reflectance spectra for nondegenerate quasi-BICs. The incident light is linearly polarized with polarization parallel to nearest neighbors depicted by the white arrow in (a). (d) Comparison between experimentally measured results and predictions from simulations for integrated reflectance.

to a complete exchange of C-point positions. This differs from the 180° rotation required to exchange the position of Dirac points with C_3 symmetry breaking deformation rotations. Again, the experimental results are in agreement with predictions from eigenpolarization simulations [Fig. 4(d)].

To quantify robustness, we fit the measured reflectively spectra with two Fano line shapes to obtain Q factors, mode positions, mode splittings, and deviations (see Supplemental Material [48]). Both cases demonstrate the potential for precisely controlling polarization while maintaining a fixed mode splitting with Q factors reaching over 200. For the C_2 symmetry breaking deformation, the average mode splitting was 22 nm with a root-mean-square deviation of only 1 nm representing a fractional variation less than 1×10^{-3} from the central wavelength. In comparison, the individual wavelengths of the upper and lower

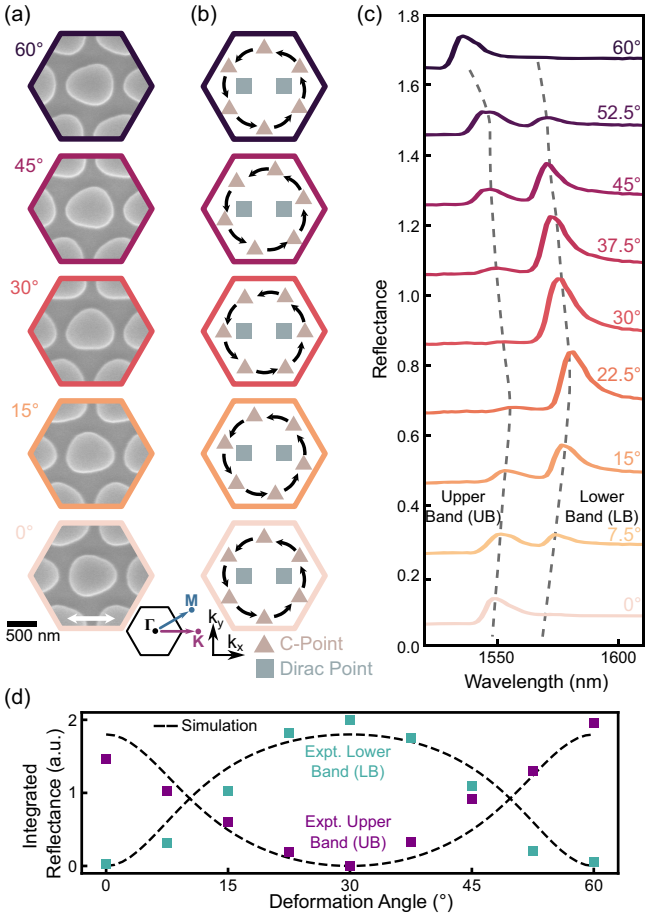

FIG. 4. (a) Scanning electron micrographs of fabricated metasurfaces and (b) schematic denoting the movement of C points when the C_2 symmetry breaking deformation angle (ψ) is swept 0° to 60°. (c) Corresponding experimentally measured reflectance spectra for nondegenerate quasi-BICs. The incident light is linearly polarized with polarization parallel to nearest neighbors depicted by the white arrow in (a). (d) Comparison between experimentally measured results and predictions from simulations for integrated reflectance.

band resonances had a root-mean-square deviation of 5 nm and 4 nm, respectively. The increased robustness of the mode splitting, relative to the resonance wavelengths, demonstrates that the mode splitting is protected by C_3 symmetry. In contrast, for devices with C_3 symmetry breaking deformation rotations, the average mode splitting was 19 nm with a root-mean-square deviation of 5 nm representing a fractional variation of 3×10^{-3} from the central wavelength. This increase in deviation can be attributed to the fact that the C_3 symmetry breaking deformation controls the mode spacing and therefore perturbations from rotating the deformation and fabrication imperfections have a larger effect.

In conclusion, we experimentally demonstrated a design paradigm for polarization control of two high-Q bands in metasurfaces through the creation, annihilation, and positioning of polarization singularities arising from symmetry-guaranteed pairs of symmetry-protected BICs. By starting with symmetry-guaranteed pairs of singularities, robust pairwise manipulation is attained, creating new pathways for harnessing polarization singularities to sculpt the far-field properties of metasurfaces for classical and quantum optics. This includes potential routes for controlled collisions between C points and Dirac points. Given that our design paradigm is rooted in group theory, its applicability expands beyond photonics. With symmetry-guaranteed pairs of symmetry-protected BICs occurring in mechanical and acoustic systems, the generality of our method may allow new means for controlling polarization singularities in acoustic and optomechanical systems [46,47].

Acknowledgments—We thank John Nogan for growing the silicon thin films used in these experiments. I. B. and C. F. D. acknowledge support from the U.S. Department of Energy, Office of Basic Energy Sciences, Division of Materials Sciences and Engineering (BES 20-017574 IB). A. C. acknowledges support from the Laboratory Directed Research and Development program at Sandia National Laboratories. This work was performed, in part, at the Center for Integrated Nanotechnologies, an Office of Science User Facility operated for the U.S. Department of Energy (DOE) Office of Science. This article has been authored by an employee of National Technology & Engineering Solutions of Sandia, LLC under Contract No. DE-NA0003525 with the U.S. Department of Energy (DOE). The DOE will provide public access to these results of federally sponsored research in accordance with the DOE Public Access Plan.

This Letter describes objective technical results and analysis. Any subjective views or opinions that might be expressed in the Letter do not necessarily represent the views of the U.S. Department of Energy or the United States Government.

[1] S. Kim, B. H. Woo, S.-C. An, Y. Lim, I. C. Seo, D.-S. Kim, S. Yoo, Q.-H. Park, and Y. C. Jun, Topological control of 2D perovskite emission in the strong coupling regime, Nano Lett. **21**, 10076 (2021).

[2] M. Kang, Z. Zhang, T. Wu, X. Zhang, Q. Xu, A. Krasnok, J. Han, and A. Alù, Coherent full polarization control based on bound states in the continuum, Nat. Commun. **13**, 4536 (2022).

[3] H. Qin, Z. Su, M. Liu, Y. Zeng, M.-C. Tang, M. Li, Y. Shi, W. Huang, C.-W. Qiu, and Q. Song, Arbitrarily polarized bound states in the continuum with twisted photonic crystal slabs, Light Sci. Appl. **12**, 1 (2023).

[4] J. Ma, J. Zhang, Y. Jiang, T. Fan, M. Parry, D. N. Neshev, and A. A. Sukhorukov, Polarization engineering of entangled photons from a lithium niobate nonlinear metasurface, Nano Lett. **23**, 8091 (2023).

[5] P. Vaity, H. Gupta, A. Kala, S. Dutta Gupta, Y. S. Kivshar, V. R. Tuz, and V. G. Achanta, Polarization-independent quasibound states in the continuum, Adv. Photonics Res. **3**, 2100144 (2022).
[6] M. Zhang, Z. Ma, M. Yang, J. Zhao, B. Wang, W. Hou, W. Zhang, C. Li, and Z. Luo, Polarization-independent multi-resonance with high q-factor for highly sensitive terahertz sensors based on all-dielectric metasurface, IEEE Photonics J. **14**, 1 (2022).
[7] X. Zhang, T. Sang, C. Pian, Y. Wang, and J. Wang, Dual-band polarization-independent high quality factor Fano resonances using a twisted tetrameric nanohole slab, J. Opt. Soc. Am. B **40**, 1652 (2023).
[8] J.-Y. Gao, J. Liu, H.-M. Yang, H.-S. Liu, G. Zeng, and B. Huang, Anisotropic medium sensing controlled by bound states in the continuum in polarization-independent metasurfaces, Opt. Express **31**, 44703 (2023).
[9] X. Sun and F. Qiu, Polarization independent high-speed spatial modulators based on an electro-optic polymer and silicon hybrid metasurface, Photonics Res. **10**, 2893 (2022).
[10] T. Wang, Z. Li, and X. Zhang, Improved generation of correlated photon pairs from monolayer WS_2 based on bound states in the continuum, Photonics Res. **7**, 341 (2019).
[11] M. Parry, A. Mazzanti, A. Poddubny, G. D. Valle, D. N. Neshev, and A. A. Sukhorukov, Enhanced generation of nondegenerate photon pairs in nonlinear metasurfaces, Adv. Opt. Photonics **3**, 055001 (2021).
[12] T. Santiago-Cruz, S. D. Gennaro, O. Mitrofanov, S. Addamane, J. Reno, I. Brener, and M. V. Chekhova, Resonant metasurfaces for generating complex quantum states, Science **377**, 991 (2022).
[13] H. Nakajima and R. Frey, Observation of bistable reflectivity of a phase-conjugated signal through intracavity nearly degenerate four-wave mixing, Phys. Rev. Lett. **54**, 1798 (1985).
[14] K. Fujita, M. Hitaka, A. Ito, M. Yamanishi, T. Dougakiuchi, and T. Edamura, Ultra-broadband room-temperature terahertz quantum cascade laser sources based on difference frequency generation, Opt. Express **24**, 16357 (2016).
[15] R. Colom, L. Xu, L. Marini, F. Bedu, I. Ozerov, T. Begou, J. Lumeau, A. E. Miroshnishenko, D. Neshev, B. T. Kuhlmey *et al.*, Enhanced four-wave mixing in doubly resonant SI nanoresonators, ACS Photonics **6**, 1295 (2019).
[16] L. Xu, D. A. Smirnova, R. Camacho-Morales, R. A. Aoni, K. Z. Kamali, M. Cai, C. Ying, Z. Zheng, A. E. Miroshnichenko, D. N. Neshev *et al.*, Enhanced four-wave mixing from multi-resonant silicon dimer-hole membrane metasurfaces, New J. Phys. **24**, 035002 (2022).
[17] E. N. Bulgakov and A. F. Sadreev, Bound states in the continuum in photonic waveguides inspired by defects, Phys. Rev. B **78**, 075105 (2008).
[18] Z. Yang, P.-S. Huang, Y.-T. Lin, H. Qin, J. Zúñiga-Pérez, Y. Shi, Z. Wang, X. Cheng, M.-C. Tang, S. Han *et al.*, Creating pairs of exceptional points for arbitrary polarization control: Asymmetric vectorial wavefront modulation, Nat. Commun. **15**, 232 (2024).
[19] F. Flossmann, O. Kevin, M. R. Dennis, and M. J. Padgett, Polarization singularities in 2D and 3D speckle fields, Phys. Rev. Lett. **100**, 203902 (2008).
[20] A. Chen, W. Liu, Y. Zhang, B. Wang, X. Liu, L. Shi, L. Lu, and J. Zi, Observing vortex polarization singularities at optical band degeneracies, Phys. Rev. B **99**, 180101(R) (2019).
[21] H. Poincaré, Mémoire sur les courbes définies par une équation différentielle, J. Math. Pures Appl. **7**, 375 (1881).
[22] H. Hopf, Vektorfelder in n-dimensionalen mannigfaltigkeiten, Math. Ann. **96**, 225 (1927).
[23] J. Milnor and D. W. Weaver, *Topology from the Differentiable Viewpoint* (Princeton University Press, Princeton, NJ, 1997), Vol. 21.
[24] B. Zhen, C. W. Hsu, L. Lu, A. D. Stone, and M. Soljačić, Topological nature of optical bound states in the continuum, Phys. Rev. Lett. **113**, 257401 (2014).
[25] J. F. Nye and M. V. Berry, Dislocations in wave trains, Proc. R. Soc. A **336**, 165 (1974).
[26] J. F. Nye and J. Hajnal, The wave structure of monochromatic electromagnetic radiation, Proc. R. Soc. A **409**, 21 (1987).
[27] M. Berry and M. Dennis, Polarization singularities in isotropic random vector waves, Proc. R. Soc. A **457**, 141 (2001).
[28] E. N. Bulgakov and A. F. Sadreev, Bound states in the continuum with high orbital angular momentum in a dielectric rod with periodically modulated permittivity, Phys. Rev. A **96**, 013841 (2017).
[29] H. M. Doeleman, F. Monticone, W. den Hollander, A. Alù, and A. F. Koenderink, Experimental observation of a polarization vortex at an optical bound state in the continuum, Nat. Photonics **12**, 397 (2018).
[30] C. Huang, C. Zhang, S. Xiao, Y. Wang, Y. Fan, Y. Liu, N. Zhang, G. Qu, H. Ji, J. Han, L. Ge, Y. Kivshar, and Q. Song, Ultrafast control of vortex microlasers, Science **367**, 1018 (2020).
[31] J. Tian, G. Adamo, H. Liu, M. Wu, M. Klein, J. Deng, N. S. S. Ang, R. Paniagua-Domínguez, H. Liu, A. I. Kuznetsov, and C. Soci, Phase-change perovskite microlaser with tunable polarization vortex, Adv. Mater. **35**, 2207430 (2023).
[32] X. Zhang, Y. Liu, J. Han, Y. Kivshar, and Q. Song, Chiral emission from resonant metasurfaces, Science **377**, 1215 (2022).
[33] A. C. Overvig, S. C. Malek, and N. Yu, Multifunctional nonlocal metasurfaces, Phys. Rev. Lett. **125**, 017402 (2020).
[34] S. C. Malek, A. C. Overvig, S. Shrestha, and N. Yu, Active nonlocal metasurfaces, Nanophotonics **10**, 655 (2020).
[35] A. Overvig, N. Yu, and A. Alù, Chiral quasi-bound states in the continuum, Phys. Rev. Lett. **126**, 073001 (2021).
[36] S. C. Malek, A. C. Overvig, A. Alù, and N. Yu, Multifunctional resonant wavefront-shaping meta-optics based on multilayer and multi-perturbation nonlocal metasurfaces, Light Sci. Appl. **11**, 246 (2022).
[37] J. R. Nolen, A. C. Overvig, M. Cotrufo, and A. Alù, Arbitrarily polarized and unidirectional emission from thermal metasurfaces, arXiv:2301.12301.
[38] B. Zhen, C. W. Hsu, Y. Igarashi, L. Lu, I. Kaminer, A. Pick, S.-L. Chua, J. D. Joannopoulos, and M. Soljačić, Spawning rings of exceptional points out of Dirac cones, Nature (London) **525**, 354 (2015).

[39] H. Zhou, C. Peng, Y. Yoon, C. W. Hsu, K. A. Nelson, L. Fu, J. D. Joannopoulos, M. Soljačić, and B. Zhen, Observation of bulk Fermi arc and polarization half charge from paired exceptional points, Science **359**, 1009 (2018).
[40] L. L. Doskolovich, E. A. Bezus, D. A. Bykov, N. V. Golovastikov, and V. A. Soifer, Resonant properties of composite structures consisting of several resonant diffraction gratings, Opt. Express **27**, 25814 (2019).
[41] L. Cong and R. Singh, Symmetry-protected dual bound states in the continuum in metamaterials, Adv. Opt. Mater. **7**, 1900383 (2019).
[42] W. Ye, Y. Gao, and J. Liu, Singular points of polarizations in the momentum space of photonic crystal slabs, Phys. Rev. Lett. **124**, 153904 (2020).
[43] Z. F. Sadrieva, I. S. Sinev, K. L. Koshelev, A. Samusev, I. V. Iorsh, O. Takayama, R. Malureanu, A. A. Bogdanov, and A. V. Lavrinenko, Transition from optical bound states in the continuum to leaky resonances: role of substrate and roughness, ACS Photonics **4**, 723 (2017).
[44] L. Ni, J. Jin, C. Peng, and Z. Li, Analytical and statistical investigation on structural fluctuations induced radiation in photonic crystal slabs, Opt. Express **25**, 5580 (2017).
[45] E. E. Maslova, M. V. Rybin, A. A. Bogdanov, and Z. F. Sadrieva, Bound states in the continuum in periodic structures with structural disorder, Nanophotonics **10**, 4313 (2021).
[46] R. D. Muelas-Hurtado, K. Volke-Sepúlveda, J. L. Ealo, F. Nori, M. A. Alonso, K. Y. Bliokh, and E. Brasselet, Observation of polarization singularities and topological textures in sound waves, Phys. Rev. Lett. **129**, 204301 (2022).
[47] S. Liu, H. Tong, and K. Fang, Optomechanical crystal with bound states in the continuum, Nat. Commun. **13**, 3187 (2022).
[48] See Supplemental Material at http://link.aps.org/supplemental/10.1103/PhysRevLett.133.213802 for additional information about experimental methods, eigenpolarization analysis techniques, and symmetry breaking operations, which includes Refs. [49–51].
[49] Y. Zeng, G. Hu, K. Liu, Z. Tang, and C.-W. Qiu, Dynamics of topological polarization singularity in momentum space, Phys. Rev. Lett. **127**, 176101 (2021).
[50] G. Son, S. Han, J. Park, K. Kwon, and K. Yu, High-efficiency broadband light coupling between optical fibers and photonic integrated circuits, Nanophotonics **7**, 1845 (2018).
[51] Z. Geng, J. Theenhaus, B. K. Patra, J.-Y. Zheng, J. Busink, E. C. Garnett, and S. R. Rodriguez, Fano lineshapes and rabi splittings: Can they be artificially generated or obscured by the numerical aperture?, ACS Photonics **8**, 1271 (2021).
[52] M. Minkov, I. A. Williamson, L. C. Andreani, D. Gerace, B. Lou, A. Y. Song, T. W. Hughes, and S. Fan, Inverse design of photonic crystals through automatic differentiation, ACS Photonics **7**, 1729 (2020).
[53] For consistency, we will use the notation of C_n referring to an element in the cyclic group and C_n referring to the group itself [54].
[54] T. Inui, Y. Tanabe, and Y. Onodera, *Group Theory and Its Applications in Physics* (Springer Science & Business Media, 2012).
[55] Additional symmetry-guaranteed pairs of symmetry-protected BICs can occur up to the diffraction limit, allowing the possibility of having pairs BICs at ω and 2ω for applications such as second harmonic generation.
[56] M. S. Dresselhaus, G. Dresselhaus, and A. Jorio, *Group Theory: Application to the Physics of Condensed Matter* (Springer Science & Business Media, Berlin, 2007).
[57] T. Yoda and M. Notomi, Generation and annihilation of topologically protected bound states in the continuum and circularly polarized states by symmetry breaking, Phys. Rev. Lett. **125**, 053902 (2020).
[58] C. F. Doiron, I. Brener, and A. Cerjan, Realizing symmetry-guaranteed pairs of bound states in the continuum in metasurfaces, Nat. Commun. **13**, 7534 (2022).